HEALTH AND MEDICINE

Glucose-responsive microneedle patch for closed-loop dual-hormone delivery in mice and pigs

Changwei Yang[1]†, Tao Sheng[1]†, Wenhui Hou[1,2], Juan Zhang[1], Li Cheng[1], Hao Wang[1], Wei Liu[1], Shiqi Wang[1], Xinmin Yu[1], Yuqi Zhang[1,3]*, Jicheng Yu[1,4,5,6]*, Zhen Gu[1,4,5,6,7]*

Insulin and glucagon secreted from the pancreas with dynamic balance play a vital role in regulating blood glucose levels. Although distinct glucose-responsive insulin delivery systems have been developed, the lack of a self-regulated glucagon release module limits their clinical applications due to the potential risk of hypoglycemia. Here, we describe a transdermal polymeric microneedle patch for glucose-responsive closed-loop insulin and glucagon delivery to achieve glycemic regulation with minimized risk of hypoglycemia. The glucose-responsive phenylboronic acid units can bind to glucose to reversibly shift the net charge (from positive to negative) of the entire polymeric matrix within microneedles. Therefore, the release ratio of the negatively charged insulin and the positively charged glucagon analog from the patch can be dynamically tuned upon the fluctuation of blood glucose levels to realize glycemic homeostasis. In both chemically induced type 1 diabetic mouse and minipig models, this glucose-responsive dual-hormone microneedle patch demonstrated tight long-term regulation in blood glucose levels (>24 hours in minipigs).

INTRODUCTION

Diabetes is a disorder of glucose metabolism that mainly occurs because of the destruction of insulin-producing β cells in the pancreas (type 1 diabetes) or peripheral insulin resistance accompanied by the decline of β cell function over time (type 2 diabetes). Diabetes has shown an increased risk of death and disability, affecting more than 537 million people worldwide (*1*, *2*). In healthy individuals, pancreatic cells tightly control fluctuations in blood glucose levels (*3*–*5*). Elevated blood glucose levels stimulate an increased insulin secretion from the pancreatic β cells, while hypoglycemia inhibits further insulin secretion (*6*) and maintains glycemic homeostasis with the secreted glucagon from the α cells (*7*). The dynamic regulation of the balance between insulin and glucagon in different situations is critical for blood glucose management.

However, the dominant treatment strategy for type 1 and advanced type 2 diabetes is still based on daily injections of exogenous insulin, which hardly satisfies the dynamic requirement of insulin and may lead to insulin-induced hypoglycemia (*8*). Although numerous glucose-responsive insulin delivery systems have been developed in the past few decades (*9*–*17*), they mainly focused on the glucose-triggered insulin delivery while challenging to maintain the dynamic balance between insulin and glucagon, which may have a substantial effect on long-term blood glucose regulation to prevent hypoglycemia.

Here, we report a glucose-responsive microneedle (MN) patch that enables closed-loop delivery of both insulin and glucagon with minimized risk of hypoglycemia for people with diabetes (Fig. 1, A and B). The glucose-responsive dual-hormone MNs (GRD-MNs) are copolymerized from a monomer mixture containing (4-((2-acrylamidoethyl) carbamoyl)-3-fluorophenyl)boronic acid (FPBA) as the glucose-responsive moiety, which can reversibly bind to glucose to generate negatively charged boronate esters. To improve the water solubility of natural glucagon and allow it to be positively charged under physiological conditions that is different from insulin, a glucagon analog (GCA) is designed in this study by the C-terminal extension with six arginine residues. The GCA and insulin are coloaded into the GRD-MNs. Upon exposure to hyperglycemia, the rapid formation of the glucose-borate complex in the FPBA unit leads to an increase in negative charge within the polymeric matrix of GRD-MNs (*18*), which reduces the electrostatic interaction of negatively charged insulin with the polymeric matrix to facilitate its rapid release into the intradermal tissue. Meanwhile, the electrostatic attraction of the polymeric matrix to positive-charged GCA is enhanced to inhibit the undesired release of GCA. By contrast, in the case of hypoglycemia, the net charge of the MNs switches from negative to positive because of the disassociation of the glucose-borate complex, which promotes the release of GCA and restrains the diffusion of insulin to restore normal blood glucose. We validated that this GRD-MN patch could mimic the glucose-dependent secretion of insulin and glucagon in the pancreas for glycemic regulation in both streptozotocin (STZ)–induced diabetic mouse and minipig models.

RESULTS

Preparation and characterization of the GRD-MN patch

The closed-loop dual-hormone MNs patch is fabricated from a mixture of *N*-vinyl pyrrolidone (NVP), *N*,*N*′-dimethylaminoethyl acrylate (DMAEA), FPBA, and ethylene dimethacrylate (EGDMA) by in situ photopolymerizations at 4°C (Fig. 1A). Among them, NVP monomer acts as a solvent for solubilizing other monomers in the matrix

[1]Key Laboratory of Advanced Drug Delivery Systems of Zhejiang Province, College of Pharmaceutical Sciences, Zhejiang University, Hangzhou 310058, China. [2]College of Bioengineering, Zhejiang University of Technology, Hangzhou 310014, China. [3]Department of Burns and Wound Center, Second Affiliated Hospital, School of Medicine, Zhejiang University, Hangzhou 310009, China. [4]Liangzhu Laboratory, Zhejiang University Medical Center, Hangzhou 311121, China. [5]Jinhua Institute of Zhejiang University, Jinhua 321299, China. [6]Department of General Surgery, Sir Run Run Shaw Hospital, School of Medicine, Zhejiang University, Hangzhou 310016, China. [7]MOE Key Laboratory of Macromolecular Synthesis and Functionalization, Department of Polymer Science and Engineering, Zhejiang University, Hangzhou 310027, China.
*Corresponding author. Email: guzhen@zju.edu.cn (Z.G.); yujicheng@zju.edu.cn (J.Y.); yqzhang21@zju.edu.cn (Y.Z.)
†These authors contributed equally to this work.

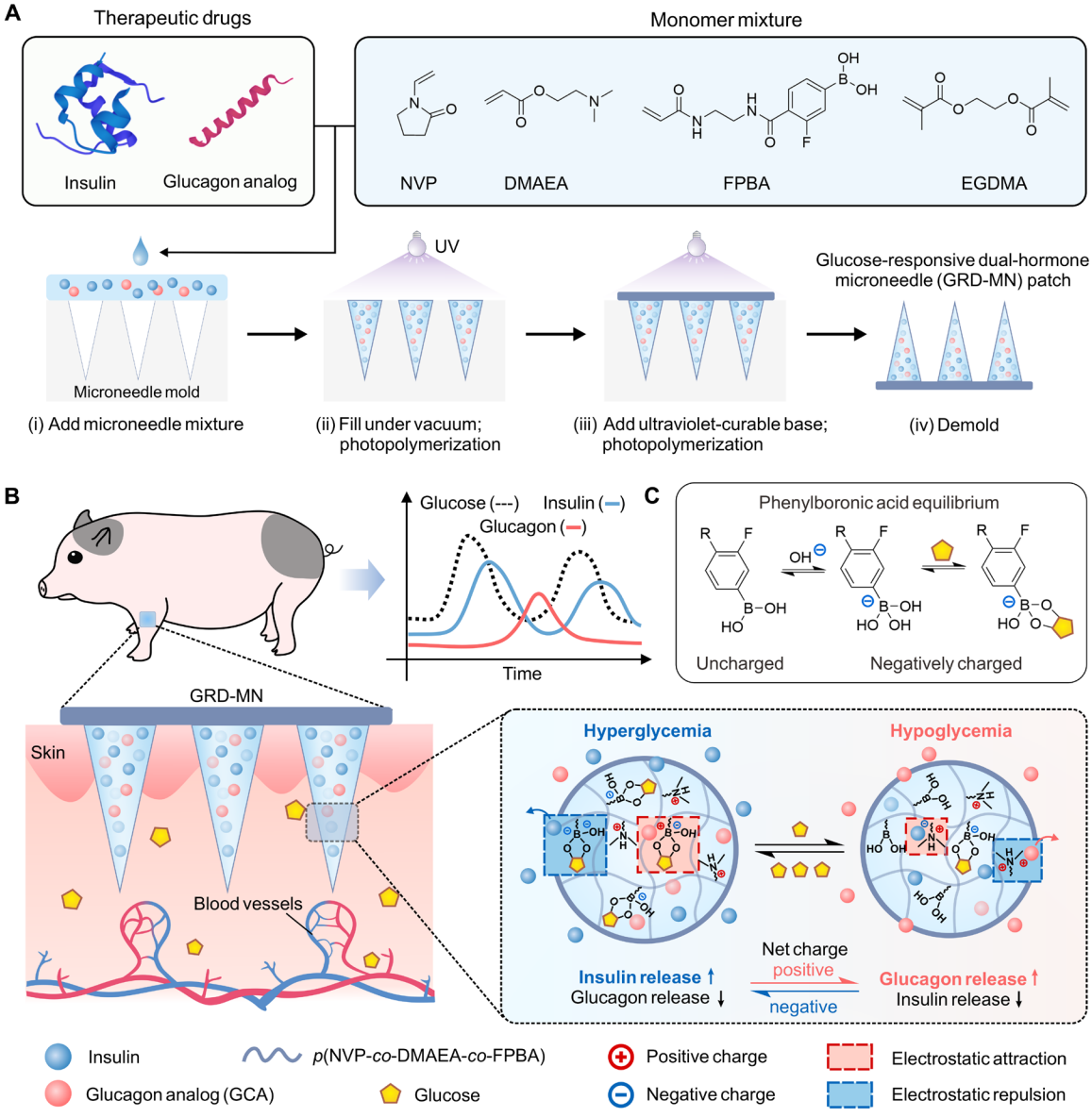

Fig. 1. Schematic of the GRD-MN patch. (**A**) Schematic of the fabrication process of the GRD-MN patch from a silicone mold using an in situ photopolymerization method. (**B**) Mechanism of glucose-triggered insulin and GCA release from GRD-MNs. Under exposure to hyperglycemia, the increased negative charge density due to the formation of the glucose-borate complex enhances electrostatic repulsion between the negatively charged insulin and the polymeric matrix, further promoting the rapid release of insulin from the MN, while the positively charged GCA is attracted to remain in the MN. In the case of hypoglycemia, the net charge of the polymeric matrix switches from negative to positive due to the disassociation of the glucose-borate complex, thus inhibiting insulin release and facilitating GCA release. Insulin and GCA release are balanced in response to blood glucose levels. (**C**) Hydrolytic equilibrium of phenylboronic acid in the presence of glucose. NVP, *N*-vinyl pyrrolidone; DMAEA, *N,N*′-dimethylaminoethyl acrylate; FPBA, (4-((2-acrylamidoethyl) carbamoyl)-3-fluorophenyl)boronic acid; EGDMA, ethylene dimethacrylate; UV, ultraviolet.

(*19*, *20*), and EGDMA monomer, the cross-linking agent, can avoid the dissolution of the polymeric matrix and improve its stiffness (*21*, *22*). Because a lower pK_a (where K_a is the acid dissociation constant) of phenylboronic acid facilitates the dynamic binding between phenylboronic acid and glucose (*23*, *24*), we chose the FPBA monomer with a low pK_a of 7.2 as the glucose-responsive unit in this study to achieve an on-demand dual-hormone release (Fig. 1C) (*25*). A representative sample of the MN patch was arranged in a 30 × 30 array (Fig. 2A); each pyramid-shaped needle was pale yellow and transparent with a width of 300 μm at the base and a height of 900 μm (Fig. 2B). In the following animal studies, the sizes of patches were further tailored to tune the insulin and GCA doses according to different animal sizes. The fluorescence image of the GRD-MN patch revealed that fluorescein isothiocyanate (FITC)–labeled insulin and rhodamine B–labeled GCA were uniformly distributed in each MN (Fig. 2C). Furthermore, such an in situ photopolymerization method allowed a nearly 100% encapsulation of insulin and GCA to achieve a high loading capability [12 and 4 weight % (wt %) for two hormones, respectively] in MNs, which is sufficient for clinical usage.

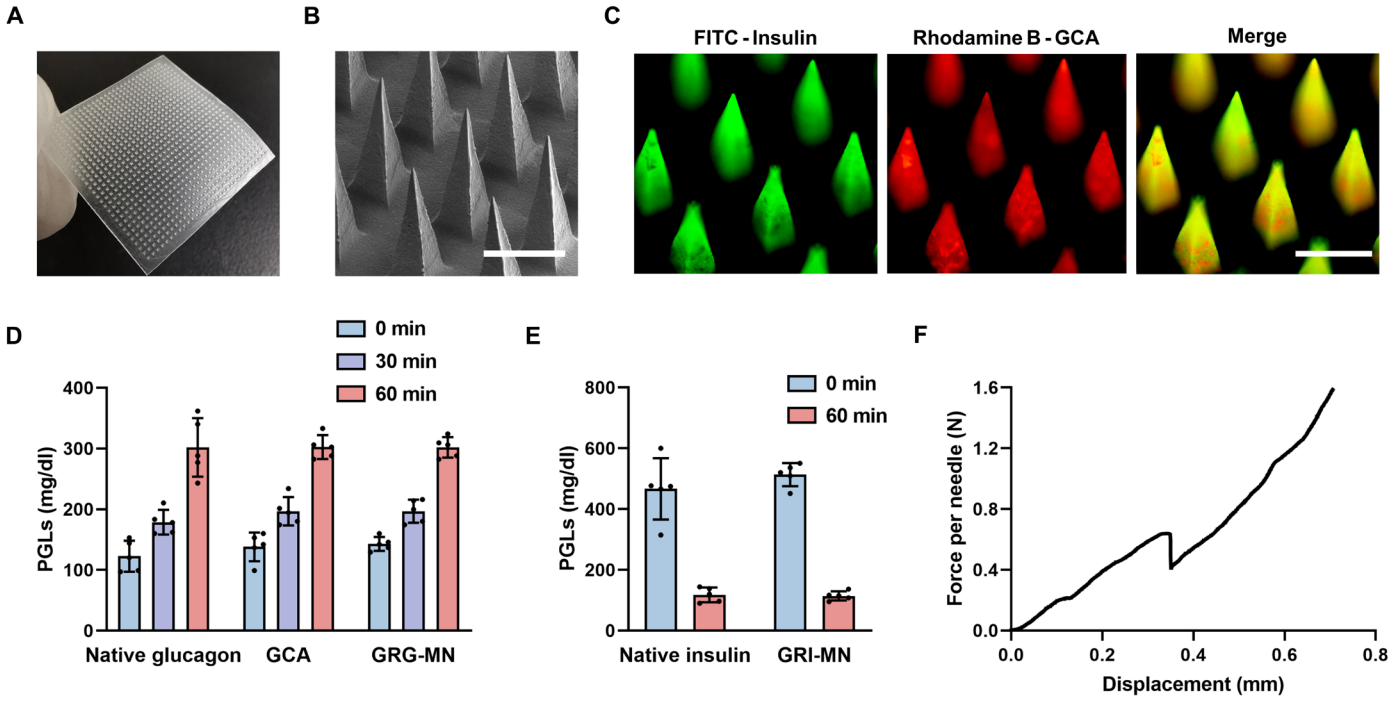

Fig. 2. Characterization of the GRD-MN patch. (**A**) Photograph of the GRD-MN patch. (**B**) Scanning electron microscopy image of the MN array. Scale bar, 500 μm. (**C**) Fluorescent images of the FITC-labeled insulin (green) and rhodamine B–labeled GCA (red) in GRD-MN. Scale bar, 500 μm. (**D**) Glucose-raising activity of native glucagon, GCA, and GCA extracted from a freshly prepared patch in insulin-administered diabetic mice. Drug dose of 0.01 mg. PGLs, plasma glucose levels; GRG-MN, glucose-responsive GCA-only MN. (**E**) Hypoglycemic activity of native insulin and insulin extracted from prepared microneedles in diabetic mice. GRI-MN, glucose-responsive insulin-only MN. (**F**) Mechanical behavior of the GRD-MNs. In (D) and (E), data are presented as means ± SD ($n = 5$).

We further assessed the glucose-raising activity of native GCA and GCA extracted from the freshly prepared glucose-responsive GCA-only MN (GRG-MN) patches and found that both of them have a similar activity to natural glucagon (Fig. 2D). Similarly, the bioactivity of insulin extracted from the resulting patches was also validated in diabetic mice (Fig. 2E). In addition, the fracture force of the GRD-MN was determined to be 0.64 ± 0.05 N per needle using a tensile compression machine (Fig. 2F), which is sufficient for skin penetration (*26*). Furthermore, it was demonstrated that the blank MNs formed by in situ photopolymerization had insignificant cytotoxicity (fig. S1).

In vitro glucose-responsive insulin and glucagon release

In the GRD-MN patch, the entire matrix of MNs with the FPBA units serves as a glucose-responsive module, which regulates the release of dual hormones through the synergistic net charge shift of the DMAEA/FPBA polymeric network at varying glucose concentrations and the difference in the isoelectric points (pIs) of two hormones at physiological pH. Under hyperglycemic conditions, the enhanced binding of glucose to FPBA units leads to an increase in the negative charge density in the polymeric matrix, facilitating negatively charged insulin (pI ~ 5.3) (*27*) release by electrostatic repulsion. In contrast, the electrostatic attraction between positively charged DMAEA units and insulin becomes the dominant force to inhibit the undesired release under hypoglycemia. As shown in Fig. 3A, a significantly fast insulin release from the glucose-responsive insulin-only MN (GRI-MN) with a DMAEA/FPBA mole ratio of 1:1.2 at high glucose level of 400 mg/dl was observed compared to other glucose concentrations. At this molar ratio, a total of 18.66 ± 1.49% (400 mg/dl), 12.36 ± 2.80% (100 mg/dl), 9.45 ± 0.88% (50 mg/dl), and 7.87 ± 0.96% (0 mg/dl) of insulin were released within 4 hours. The glucose-dependent release behavior was hampered by varying the DMAEA/FPBA ratios due to the excess positive or negative charges within the matrix (fig. S2). In opposite to insulin, the GCA, by introducing six arginine residues to the C terminus of natural glucagon, has a higher pI of 12.4 (fig. S3), thus having positive charges at pH 7.4. Therefore, the release of GCA from the GRG-MN was inhibited under hyperglycemia because of its electrostatic attraction to the negatively charged glucose-borate complex, while it showed a quick release under hypoglycemia (Fig. 3B). It was observed that a total of 12.22 ± 3.39% (400 mg/dl), 13.16 ± 2.67% (100 mg/dl), 20.30 ± 4.15% (50 mg/dl), and 31.08 ± 2.67% (0 mg/dl) of GCA were released within 4 hours.

We further assessed the release profiles for both insulin and GCA from the GRD-MN patches at varying glucose concentrations. As shown in Fig. 3 (C and D), the glucose-dependent release performance of the two hormones was similar to the release behavior of their individual loaded MNs. Note that the GRD-MN patches were able to efficiently tune the ratios of the release rates between insulin and GCA at different glucose levels (Fig. 3E), which is crucial for glycemic homeostasis (*28*). Moreover, the pulsatile release profiles for the GRD-MN patches demonstrated that the glucose-responsive hormone release could be achieved for several cycles by alternately incubating the polymeric matrix in low-glucose (50 mg/dl) and high-glucose (400 mg/dl) solutions (Fig. 3, F and G). Notably, MNs as drug delivery carriers can improve the stability and protect the activity of protein drugs at room temperature. Both insulin and GCA in the GRD-MN patches maintained their bioactivity for at least 3 months (Fig. 3, H and I).

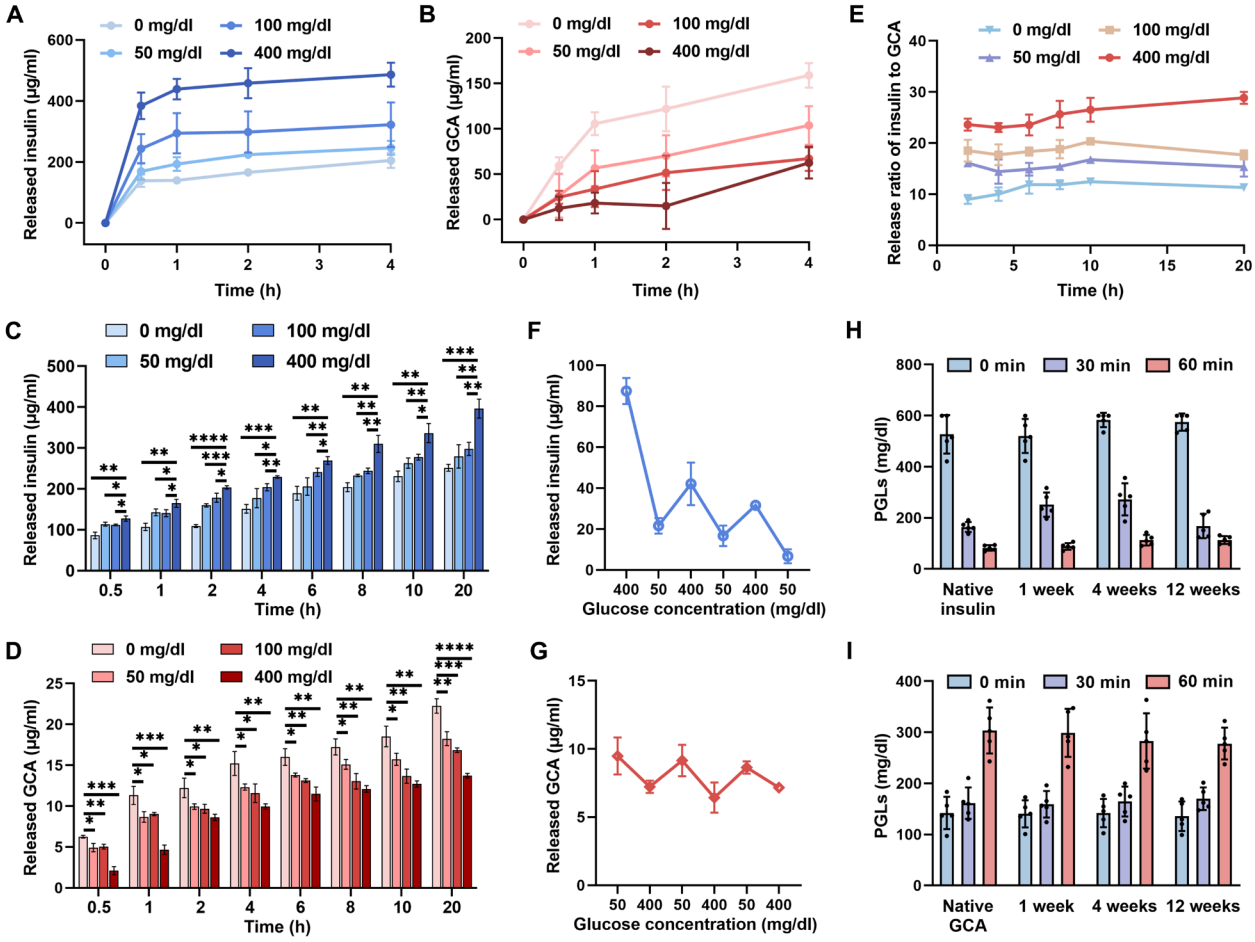

Fig. 3. In vitro evaluation of the GRD-MN patch. (**A**) In vitro accumulated insulin release from GRI-MN patch in varying glucose concentrations ($n = 3$). (**B**) In vitro accumulated GCA release from GRG-MN patch in varying glucose concentrations ($n = 3$). (**C** and **D**) Glucose-responsive release of insulin (**C**) and GCA (**D**) from the GRD-MN patch in different glucose concentrations. (**E**) Release ratio of insulin to GCA from GRD-MN calculated according to the results in (C) and (D). (**F** and **G**) Pulsatile release of insulin (F) and GCA (G) by alternating the glucose concentrations between 50 and 400 mg/dl. The incubation time for insulin and GCA in each circle is 30 min ($n = 3$). (**H**) Hypoglycemic activity of the insulin extracted from the patches stored at room temperature in diabetic mice ($n = 5$). Insulin dose of 0.05 mg. (**I**) Glucogenic activity of the GCA extracted from the patches stored at room temperature in hypoglycemic mice ($n = 5$). GCA dose of 0.01 mg. Data are presented as means ± SD. $^{*}P < 0.05$, $^{**}P < 0.01$, $^{***}P < 0.001$, and $^{****}P < 0.0001$.

In vivo studies in an STZ-induced diabetic mouse model

The capacity of the GRD-MN patches to penetrate the skin was first confirmed by the generation of microchannels on the skin and subsequent trypan blue staining result (Fig. 4A). In addition, scanning electron microscopy (SEM) imaging of the GRD-MN patches before and after administration on mice skin revealed that there were insignificant breakage and defects of MNs (fig. S4), indicating its good clinical safety.

Afterward, we assessed the in vivo performance of the GRD-MN patch in an STZ-induced type 1 diabetic mouse model. Diabetic mice were randomly assigned to groups and transcutaneously treated with either GRD-MN patches or GRI-MN patches. Meanwhile, mice treated with subcutaneous injections of insulin solution and phosphate-buffered solution (PBS) solution were set up as controls. The plasma glucose levels (PGLs) in treated mice were measured over time. The PGLs of the mice dropped below 200 mg/dl (normoglycemic levels) in both patch-treated groups (Fig. 4B). Notably, the diabetic mice treated with the GRD-MN patch maintained normal blood glucose levels for up to 9 hours with no hypoglycemic events under the normal diet condition, while the GRI-MN patch group had individual cases of hypoglycemia (blood glucose below 50 mg/dl) 4 hours after administration. Respectively, plasma insulin levels rapidly increased at hyperglycemia and maintained at basal release rate during normoglycemia in the GRD-MN group, and GCA was slowly released at both hyperglycemia and normoglycemia, consistent with well glycemic regulation (Fig. 4C).

Subsequently, we performed an intraperitoneal glucose tolerance test (IPGTT) at 3 hours after administration of the patches, in which the glucose dose was 1.5 g/kg, to evaluate the glucose regulation capacity of the GRD-MN patch. After a glycemic peak, the PGLs in both healthy mice and diabetic mice exposed to the GRD-MN patches returned to normoglycemia, while the mice exposed to the subcutaneous insulin injection showed a steady increase in glucose levels over 120 min (Fig. 4, D and E). To further confirm insulin release induced by hyperglycemia in vivo, we conducted a glucose tolerance test with a higher dose of 3 g/kg on diabetic mice 3 hours after the GRD-MN patch was administrated. A spike in plasma insulin levels occurred following the elevation of glucose levels, indicating

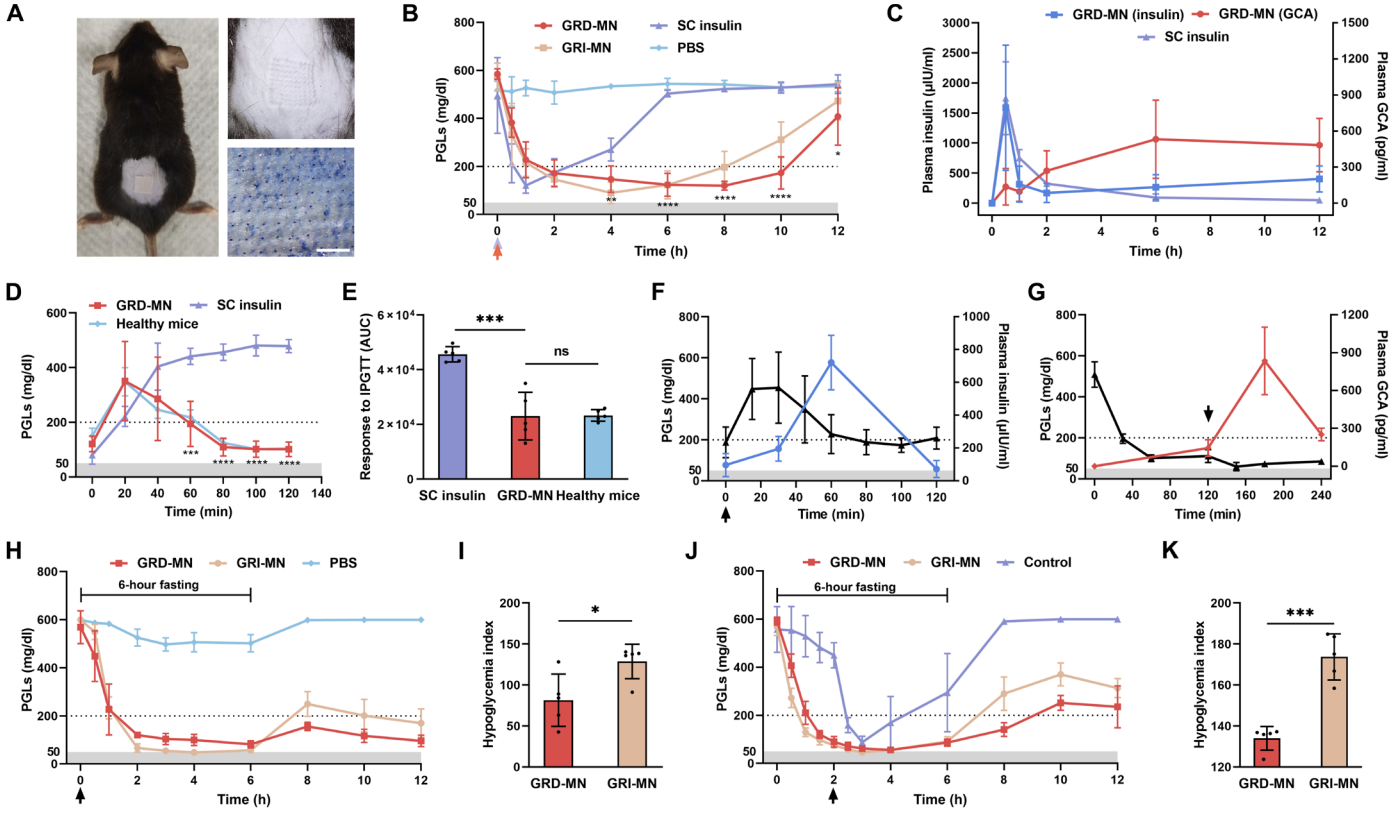

Fig. 4. In vivo evaluation of the GRD-MN patch in an STZ-induced diabetic mice model. (**A**) A diabetic mouse was treated with the GRD-MN patch (left). MN traces on skin (right top). Trypan blue–stained skin (right bottom). Scale bar, 2 mm. (**B** and **C**) PGLs (B) and plasma human insulin/GCA concentrations (C) in diabetic mice treated with PBS, insulin solution (purple arrow; insulin dose of 0.05 mg), the GRI-MN, or GRD-MN (the orange arrow). SC, subcutaneous. (**D**) Intraperitoneal glucose tolerance test (IPGTT) at 3 hours after administration of GRD-MN or insulin injection. Insulin dose of 0.05 mg. Glucose dose of 1.5 g/kg. (**E**) Responsiveness was calculated on the basis of the area under the curve (AUC) from 0 to 120 min. ns, not significant. (**F**) In vivo glucose-responsive insulin release stimulated by intraperitoneal glucose challenge (black arrow) 3 hours after GRD-MN administration. Glucose dose of 3 g/kg. (**G**) Hypoglycemia-triggered GCA release, promoted by insulin injection (black arrow) at 2 hours after administration of GRD-MN. Insulin dose of 500 μg/kg. (**H** and **I**) PGLs (H) and hypoglycemia index (I) in diabetic mice fasted for 6 hours after the GRI-MN or GRD-MN patches administration (black arrow). (**J** and **K**) PGLs (J) and hypoglycemia index (K) of diabetic mice injected with insulin (50 μg/kg) 2 hours (black arrow) after administration of GRI-MN or GRD-MN patches. In (B), (D), (F), (G), (H), and (J), the severe hypoglycemia region (<50 mg/dl) is shown in the shaded area. GRI-MN: insulin dose of 0.729 mg. GRD-MN: insulin dose of 0.729 mg and GCA dose of 0.243 mg. Data are presented as means ± SD ($n = 5$). Statistical analysis was all performed using a two-tailed Student's *t* test [comparison between the GRD-MN and subcutaneous insulin groups in (B) and the GRD-MN and subcutaneous insulin groups in (D)]. $^{*}P < 0.05$, $^{**}P < 0.01$, $^{***}P < 0.001$, and $^{****}P < 0.0001$.

that the GRD-MN patch has rapid hyperglycemic responsiveness (Fig. 4F).

To confirm the capability of the GRD-MN to mitigate hypoglycemia, the insulin-overdosing hypoglycemic diabetic mice were treated with the GRD-MN patch under fasting conditions. With the treatment of the GRD-MN patch, the mice quickly restored normoglycemia, while the GRI-MN–treated group still remained in hypoglycemia (fig. S5). In addition, the in vivo hypoglycemia-triggered release of GCA was also substantiated in a subcutaneous injection insulin challenge test (Fig. 4G). To further evaluate the antihypoglycemic capacity of the GRD-MN patch, diabetic mice treated with GRI-MN and GRD-MN patches were kept under fasting conditions to simulate the situation of a delayed meal. As shown in Fig. 3H, the GRD-MN patch was able to maintain PGLs within the normal range, whereas the mice treated with the GRI-MN patches showed hypoglycemia during 4 to 6 hours after administration (Fig. 4, H and I). Furthermore, even with a sudden overdosing of insulin (0.5 mg/kg, subcutaenously), the GRD-MN patch could still keep PGLs in the normal range, whereas hypoglycemia occurred in the mice with the GRI-MN patch (Fig. 4, J and K). Upon resumption of feeding, the GRI-MN–treated group showed a faster rise in blood glucose than the GRD-MN–treated group, which may be explained by the reduced appetite due to glucagon (*29*, *30*).

In vivo studies in an STZ-induced diabetic minipig model

To further assess the clinical potential of the GRD-MN patch, we established an STZ-induced insulin-deficient minipig model because the general structure, thickness, hair thinning, collagen, and lipid composition of porcine skin are highly similar to the human skin (Fig. 5A) (*31*). The diabetic minipigs were transcutaneously treated with the GRD-MN patch or a subcutaneous insulin injection. The continuous glucose monitoring systems (CGMSs; Abbott) were applied to the minipigs for the real-time and sustained recording of PGLs. The results indicated that PGLs in GRD-MN–treated pigs sustainably decreased to normoglycemia in the first 2 hours and maintained normoglycemic levels with slight fluctuations for up to 24 hours until intake of the meal on the next day (Fig. 5, B to E). In contrast, PGLs of the minipigs injected with insulin quickly dropped

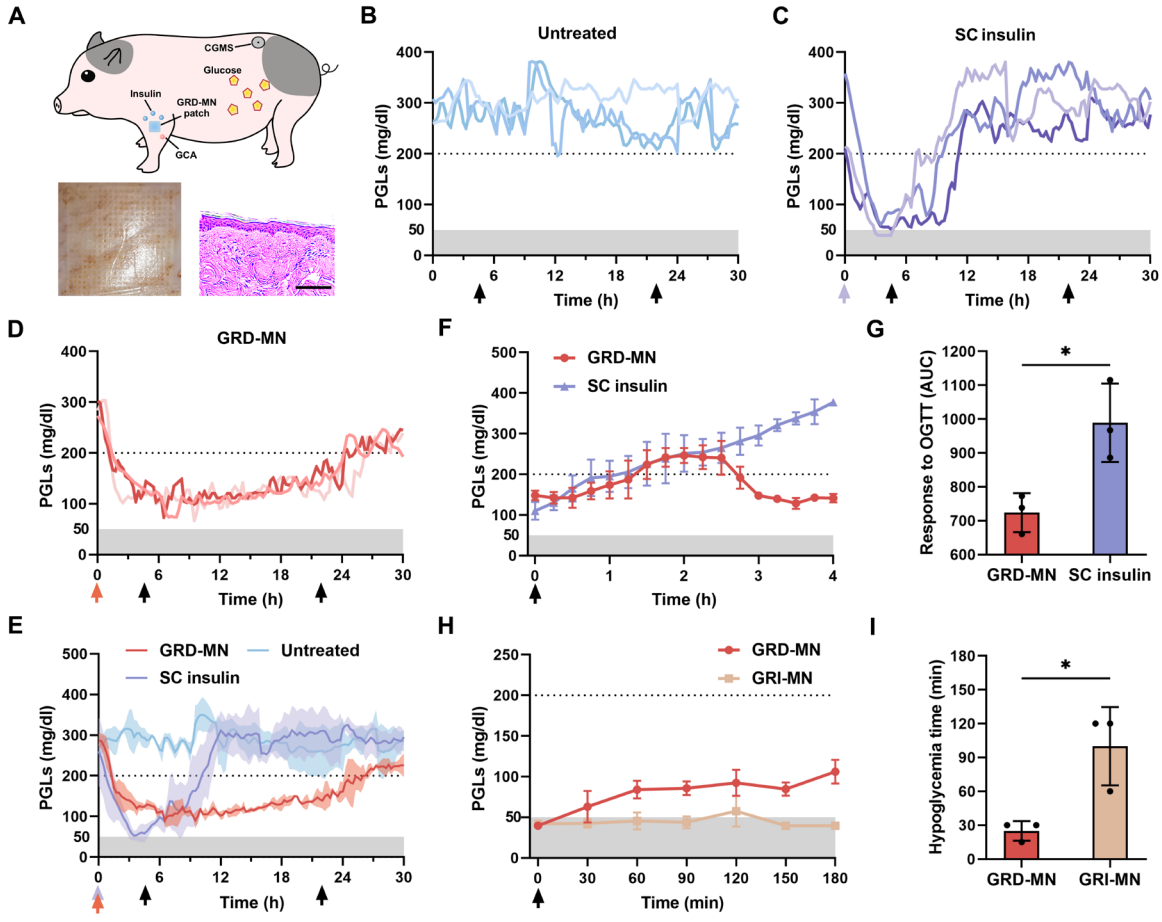

Fig. 5. In vivo evaluation of the GRD-MN patch in an STZ-induced diabetic minipigs model. (**A**) Top: Schematic of a minipig treated with GRD-MN at the leg site and monitored with a CGMS. Bottom left: Photograph of a GRD-MN patch applied on the minipig leg. Bottom right: H&E staining section of skin of minipigs after treatment of the GRD-MN patch. Scale bar, 50 μm. (**B** to **D**) Individual PGLs in STZ-induced diabetic minipigs without treatment (B), treated with insulin injection (insulin dose of 0.12 IU/kg) (C), and treated with GRD-MN (D). (**E**) Average PGLs in diabetic minipigs with different treatments. The orange arrow, purple arrow, and black arrows indicate the time point of the MN patch administration, subcutaneous insulin injection, and feeding, respectively. (**F**) Oral glucose tolerance test in diabetic minipigs at 3 hours after administration of GRD-MN or subcutaneous insulin injection (insulin dose of 0.12 IU/kg). Glucose dose of 1 g/kg. The time point of glucose feeding was indicated by black arrow. (**G**) Responsiveness was calculated on the basis of the area under the curve from 0 to 4 hours, and the baseline was set at the plasma glucose readings (0 min). (**H**) In vivo insulin-triggered antihypoglycemia test. The diabetic minipigs received subcutaneous insulin injection challenge and then treated with GRD-MN or GRI-MN (black arrow) 2 hours after injection, respectively. Insulin dose of 0.4 IU/kg. (**I**) Hypoglycemic duration of diabatic minipigs treated with GRI-MN and GRD-MN. The administration time point of patches was set to 0 min. Statistical significance was determined by a two-tailed Student's *t* test. GRD-MN: insulin dose of 4.8 mg and GCA dose of 1.6 mg. GRI-MN: insulin dose of 4.8 mg. In (F) to (I), data are presented as means ± SD ($n = 3$). *$P < 0.05$.

within 2 hours, while they increased to hyperglycemia just after one meal (Fig. 5C).

An oral glucose tolerance test (OGTT) was further performed at 4 hours after treatment with the GRD-MN patches or subcutaneous injection of insulin. Unlike the minipigs that received insulin injection, the rapidly elevated PGLs in minipigs treated with the GRD-MN patch could be suppressed and subsequently returned to normoglycemic levels (Fig. 5, F and G). Moreover, a subcutaneous insulin tolerance test (SITT) was also performed to verify the emergency effect of the GRD-MN patch on hypoglycemia in minipigs. Consistent with the hypoglycemic mice model, the PGLs of the insulin-induced hypoglycemic minipigs with the GRD-MN patches under the fasting state rapidly recovered to the normoglycemic condition (Fig. 5, H and I), indicating that the GRD-MN patch could effectively alleviate the hypoglycemic period compared to the GRI-MN patch. In addition, insignificant inflammation was observed in the skin tissue administered with patches from the hematoxylin and eosin (H&E) staining results (fig. S6).

DISCUSSION

Glucose-responsive closed-loop delivery systems mimicking the function of the pancreas hold great promise for tight regulation of blood glucose in people with diabetes. During the past few decades, substantial efforts have been made to the development of glucose-responsive insulin delivery strategies, and the "smart insulin patch" has been entering clinical trial (*32*). Nonetheless, little attention has been devoted to the significance of the integration of the glucose-responsive glucagon delivery with closed-loop insulin delivery to achieve a dynamic balance of these two essential hormones for glycemic regulation.

To this end, we developed a glucose-responsive MN array patch loaded with both insulin and glucagon as the closed-loop dual-hormone delivery system for daily management of diabetes with minimized risk of hypoglycemia. Although glucose-triggered glucagon delivery has been reported to reduce the risk of hypoglycemia (*33*), the development of the glucose-dependent insulin and glucagon co-delivery system still remains challenging. Compared to our previous study on a hybrid patch with two modules for glucose-responsive insulin and glucagon delivery, respectively (*17*), these two hormones can be incorporated into the same module, and the preparation process of GRD-MN patches is simple and feasible for mass production, which is significant for clinical translation. Taking advantages of the glucose-mediated switch in the net charge of the MN polymeric matrix induced by the reversible interaction between FPBA and glucose, the release rates of negatively charged insulin and positively charged GCA from the GRD-MN patches could be adjusted according to the variable electrostatic interaction. The release ratios of insulin to glucagon have been validated to be tuned in a glucose-dependent manner in vitro.

The in vivo studies in the type 1 diabetic mouse model further substantiated that the GRD-MN patches could mimic the function of pancreatic islets to achieve robust glycemic control with the capacity to prevent hypoglycemia. Moreover, the long-term glucose regulation over 24 hours was also demonstrated in type 1 diabetic minipigs with the normal feeding frequency, verifying the closed-loop delivery of dual hormones from GRD-MNs. Moreover, this closed-loop delivery strategy for two drugs with opposing actions could be further expanded to regulate physiological homeostasis for the treatments of other diseases.

MATERIALS AND METHODS

Materials

All chemicals were purchased from Aladdin unless otherwise specified and were used as received. Norland Optical Adhesive was purchased from Norland Products Inc. Human recombinant insulin was purchased from Solarbio (catalog no. I8830). GCA was purchased from GL Biochem. Human glucagon was purchased from Bidet Pharmaceuticals (catalog no. BD132093). Coomassie Plus Protein Assay Reagent was purchased from Thermo Scientific (catalog no. 23236). FPBA was purchased from Ambeed (catalog no. A1194179). STZ was purchased from Macklin (catalog no. S817944).

Preparation of insulin and GCA dual-hormone MN patches

The GRD-MN patch was prepared by mold-based polymerization under ultraviolet (UV) irradiation. First, insulin (12 wt %) and GCA (4 wt %) were preloaded in the NVP monomer liquid containing EGDMA (1.5 wt %) as the cross-linking agent and 2-hydroxy-4′-(2-hydroxyethoxy)-2-methylpropiophenone (Irgacure 2959; 1.5 wt %) as the photoinitiator, as well as FPBA and DMAEA at a molar ratio of 1.2. Afterward, the mixture was pipette-applied to the mold surface and then vacuum-infiltrated into the MN mold. The excess solution was removed from the mold surface before photopolymerization under a UV lamp (2 W/cm^2; 365 nm) for 1 min at 4°C. Then, the UV-curable material (Norland Optical Adhesive) was dropped on the mold to form the base of the patch. After being cured under UV light (6 W/cm^2; 365 nm) for 15 min, the resulting patch was carefully detached from the mold, which was kept dry at room temperature for further study. The insulin-only (12 wt %) or GCA-only (4 wt %) MN patches were prepared in the same way.

Characterizations of the MN patches

The fluorescent images of the MNs were observed using a fluorescent microscope (ECLIPSE Ti2-U, Nikon). The SEM images of the MN patch were obtained by Nova Nano 450 field emission scanning electron microscope. The patch was sputtered with a gold/palladium target for 30 s before imaging. The mechanical strength of the MNs was determined by pressing them against a stainless steel plate. The initial gauge was set to 5.00 mm between the MN tips and the stainless steel plate, and the load cell capacity was 50.00 N. The upper stainless steel plate moved at a rate of 1.00 mm/min toward the MN. The failure force of the MNs at the beginning of needle bending was recorded.

H&E staining of skin sections

The GRD-MN patches were applied to the shaved back of the mice and minipigs for 12 hours. After MN removal for 2, 24, and 72 hours (for mice) or 1, 3, and 5 days (for minipigs), animals were euthanized, and then, pieces of skin from the treated sites were harvested and fixed in 4% formaldehyde for 24 hours before H&E staining. The images were taken using a microscope (Olympus).

Cytotoxicity study

The cytotoxicity assay for GRD-MN patches was performed according to the protocol of the CCK-8 Kit (Tong Ren, Japan). B16F10 cells were spread in 96-well plates at a density of 5000 cells per well. Drug-free MNs were placed in the medium until the water absorption was completely swollen, followed by placing the MNs in the transwell plate, adding the medium to the 96-well plate, and incubating for 24 hours. The transwell plate was removed, and the CCK-8 solution was added to each well and incubated for another 4 hours. The absorbance was detected at 450 nm on the Synergy H1 Microplate Reader (BioTek).

In vitro release studies

To evaluate the glucose-responsive release of insulin or GCA, the GRI-MN and GRG-MN patch samples were incubated in 1 ml of PBS solutions (pH 7.4) with varying glucose concentrations (0, 50, 100, and 400 mg/dl) at 37°C with gentle shaking. At predetermined time points, 10 μl of the supernatant was collected into a 96-well plate, and the released insulin or GCA was quantified using a Coomassie (Bradford) protein assay. The absorbance was detected at 595 nm on the Synergy H1 Microplate Reader (BioTek), and the concentration was calculated with insulin (10 to 600 μg/ml) or glucagon (10 to 200 μg/ml) standard curve. The release behavior of the FITC-labeled insulin and rhodamine B–labeled GCA from the GRD-MN patches was determined in the same way. The release of insulin (excitation wavelength of 490 nm and emission wavelength of 520 nm) and GCA (excitation wavelength of 540 nm and emission wavelength of 592 nm) were detected by fluorescence intensity. The concentration was calculated with FITC-labeled insulin (1 to 500 μg/ml) or rhodamine B–labeled GCA (1 to 100 μg/ml) standard curve. All experiments were repeated three times.

In vivo studies in STZ-induced diabetic mice

All animal experiments were performed in compliance with an animal study protocol approved by the Animal Committee of Zhejiang University. We examined the therapeutic impact of the GRD-MN

patch on diabetic mice according to the previously reported approach (*16*). The in vivo performance of the patches was evaluated on STZ-induced adult diabetic mice (male C57BL/6; weight, 20 to 25 g; Zhejiang University Animal Experiment Center). For MN application on mice, the patch was pressed firmly for 10 s and immobilized on the skin of mice by applying a medical tape. After insertion, the PGLs were recorded with an Accu-Chek Aviva glucometer (Roche Diabetes Care Inc.). The patches used for mice had a 15 × 15 array of MNs of pyramidal shape, with a width of 300 μm at the base and a height of 900 μm.

The plasma insulin level was measured by collecting 20 μl of plasma, which was stored at −20°C until measurement using a human insulin enzyme-linked immunosorbent assay (ELISA) kit (catalog no. E-EL-H2665c, Elabscience) according to the manufacturer's instruction. The plasma concentrations of rhodamine B–labeled GCA were measured on the Synergy H1 Microplate Reader (BioTek). For IPGTT-triggered insulin release, diabetic mice were treated with the GRD-MN patch (insulin dose of 0.729 mg and GCA dose of 0.243 mg). Intraperitoneal glucose (0.3 g/ml in PBS) was given 3 hours after treatment at a dose of 3 or 1.5 g/kg to achieve an increased peak in blood glucose level, and PGLs were measured with an Accu-Chek Aviva blood glucose meter through the tail vein blood (~3 μl). For plasma insulin quantification, the blood was collected (~50 μl) at predetermined intervals, centrifuged to isolate plasma, and stored at −20°C until measurement with an ELISA kit.

For intraperitoneal insulin tolerance test–triggered GCA release, diabetic mice were treated with the GRD-MN patch (insulin dose of 0.729 mg and GCA dose of 0.243 mg). Intraperitoneal insulin (1 mg/ml in PBS) was given 2 hours after treatment at a dose of 0.5 mg/kg to achieve an insulin-induced hypoglycemia. PGLs were measured with the glucometer. For plasma GCA quantification, the blood was collected (~50 μl) at predetermined intervals to isolate plasma for measurement with the fluorescence detection method.

In vivo studies in STZ-induced diabetic minipigs

The animal study protocol was approved by the Animal Committee of Zhejiang University. The in vivo studies on diabetic minipigs were performed according to our previously reported approach (*16*). Three male Bama minipigs (Shanghai Jiagan Biotechnology Co. Ltd.) were used. Diabetes was induced in minipigs by infusion of STZ (150 mg/kg). STZ was dissolved in freshly prepared disodium citrate buffer (pH 4.5) at a concentration of 75 mg/ml and administered intravenously within 15 min. After 7 days of recovery, the successful establishment of an insulin-deficient diabetic model was confirmed by monitoring glucose levels using CGMS (FreeStyle Libre H, Abbott). Diabetic minipigs were treated with insulin (0.3 to 0.8 U/kg) once daily to control blood glucose, and daily treatment was stopped 24 hours before the experiment to reduce the effect of remaining insulin. PGL was monitored continuously using CGMS, and meals were provided twice daily for the duration of the experiment or as needed for the experiment. The CGMS was calibrated according to the manufacturer's manual during the experiment by measuring the plasma glucose using a Clarity GL2PLUS glucose meter. For MN application on minipigs, the minipigs were treated transcutaneously with the GRD-MN patches (insulin dose of 4.8 mg and GCA dose of 1.6 mg) at the leg sites for each pig. The patches used for minipigs had a 20 × 20 array of MNs of pyramidal shape, with a width of 500 μm at the base and a height of 1200 μm.

An OGTT was conducted on diabetic minipigs to evaluate the glucose-responsive capability of the GRD-MN patches. All minipigs were fasted overnight before administration. The minipigs were transcutaneously treated with the GRD-MN patches at the leg site. A glucose solution was administered orally to the minipigs 4 hours after treatment at a dose of 1 g/kg. The PGLs were continuously monitored using the CGMS.

For SITT-triggered antihypoglycemia in diabetic minipigs, insulin (0.1 IU/kg) was given at 2 hours before the GRD-MN patch (insulin dose of 4.8 mg and GCA dose of 1.6 mg) or GRI-MN patch (insulin dose of 4.8 mg) administration to achieve an insulin-induced hypoglycemia. PGLs were measured with the CGMS.

Statistical analysis

All the results are presented as means ± SD. Statistical analysis was performed using a two-tailed Student's *t* test for two-group comparisons. All statistical analyses were performed using the Prism software package (Prism version 7.0d, GraphPad Software, USA, 2017). The differences between experimental and control groups were considered statistically significant at $P < 0.05$. Significance is denoted in the figures as $^{*}P < 0.05$, $^{**}P < 0.01$, $^{***}P < 0.001$, and $^{****}P < 0.0001$.

SUPPLEMENTARY MATERIALS

Supplementary material for this article is available at https://science.org/doi/10.1126/sciadv.add3197

View/request a protocol for this paper from *Bio-protocol*.

REFERENCES AND NOTES

1. Y. Ohkubo, H. Kishikawa, E. Araki, T. Miyata, S. Isami, S. Motoyoshi, Y. Kojima, N. Furuyoshi, M. Shichiri, Intensive insulin therapy prevents the progression of diabetic microvascular complications in Japanese patients with non-insulin-dependent diabetes mellitus: A randomized prospective 6-year study. *Diabetes Res. Clin. Pract.* **28**, 103–117 (1995).
2. O. Veiseh, B. C. Tang, K. A. Whitehead, D. G. Anderson, R. Langer, Managing diabetes with nanomedicine: Challenges and opportunities. *Nat. Rev. Drug Discov.* **14**, 45–57 (2015).
3. G. B. Bolli, P. D. Feo, S. D. Cosmo, G. Perriello, M. M. Ventura, F. Calcinaro, C. Lolli, P. Campbell, P. Brunetti, J. E. Gerich, Demonstration of a dawn phenomenon in normal human volunteers. *Diabetes* **33**, 1150–1153 (1984).
4. E. VanCauter, K. S. Polonsky, A. J. Scheen, Roles of circadian rhythmicity and sleep in human glucose regulation. *Endocr. Rev.* **18**, 716–738 (1997).
5. A. Kalsbeek, C. X. Yi, S. E. La Fleur, E. Fliers, The hypothalamic clock and its control of glucose homeostasis. *Trends Endocrinol. Metab.* **21**, 402–410 (2010).
6. J. H. Koeslag, P. T. Saunders, E. Terblanche, A reappraisal of the blood glucose homeostat which comprehensively explains the type 2 diabetes mellitus-syndrome X complex. *J. Physiol.* **549**, 333–346 (2003).
7. P. V. Roder, B. B. Wu, Y. X. Liu, W. P. Han, Pancreatic regulation of glucose homeostasis. *Exp. Mol. Med.* **48**, e219 (2016).
8. M. R. Prausnitz, R. Langer, Transdermal drug delivery. *Nat. Biotechnol.* **26**, 1261–1268 (2008).
9. V. Lassmann-Vague, D. Raccah, Alternatives routes of insulin delivery. *Diabetes Metab.* **32**, 513–522 (2006).
10. K. Podual, F. J. Doyle III, N. A. Peppas, Preparation and dynamic response of cationic copolymer hydrogels containing glucose oxidase. *Polymer* **41**, 3975–3983 (2000).
11. E. Cengiz, J. L. Sherr, S. A. Weinzimer, W. V. Tamborlane, New-generation diabetes management: Glucose sensor-augmented insulin pump therapy. *Expert Rev. Med. Devices* **8**, 449–458 (2011).
12. H. C. Yeh, T. T. Brown, N. Maruthur, P. Ranasinghe, Z. Berger, Y. D. Suh, L. M. Wilson, E. B. Haberl, J. Brick, E. B. Bass, S. H. Golden, Comparative effectiveness and safety of methods of insulin delivery and glucose monitoring for diabetes mellitus a systematic review and meta-analysis. *Ann. Intern. Med.* **157**, 336–347 (2012).
13. S. Mitragotri, P. A. Burke, R. Langer, Overcoming the challenges in administering biopharmaceuticals: Formulation and delivery strategies. *Nat. Rev. Drug Discov.* **13**, 655–672 (2014).
14. J. Yu, Y. Zhang, H. Bomba, Z. Gu, Stimuli-responsive delivery of therapeutics for diabetes treatment. *Bioeng. Transl. Med.* **1**, 323–337 (2016).
15. J. T. Warshauer, J. A. Bluestone, M. S. Anderson, New frontiers in the treatment of type 1 diabetes. *Cell Metab.* **31**, 46–61 (2020).

16. J. Yu, J. Wang, Y. Zhang, G. Chen, W. Mao, Y. Ye, A. R. Kahkoska, J. B. Buse, R. Langer, Z. Gu, Glucose-responsive insulin patch for the regulation of blood glucose in mice and minipigs. *Nat. Biomed. Eng.* **4**, 499–506 (2020).
17. Z. J. Wang, J. Wang, H. Li, J. Yu, G. Chen, A. R. Kahkoska, V. Wu, Y. Zeng, D. Wen, J. R. Miedema, J. B. Buse, Z. Gu, Dual self-regulated delivery of insulin and glucagon by a hybrid patch. *Proc. Natl. Acad. Sci. U.S.A.* **117**, 29512–29517 (2020).
18. J. Wang, Z. Wang, J. Yu, A. R. Kahkoska, J. B. Buse, Z. Gu, Glucose-responsive insulin and delivery systems: Innovation and translation. *Adv. Mater.* **32**, e1902004 (2020).
19. S. P. Sullivan, N. Murthy, M. R. Prausnitz, Minimally invasive protein delivery with rapidly dissolving polymer microneedles. *Adv. Mater.* **20**, 933–938 (2008).
20. S. P. Sullivan, D. G. Koutsonanos, M. del Pilar Martin, J. W. Lee, V. Zarnitsyn, S.-O. Choi, N. Murthy, R. W. Compans, I. Skountzou, M. R. Prausnitz, Dissolving polymer microneedle patches for influenza vaccination. *Nat. Med.* **16**, 915–920 (2010).
21. T. Tamai, P. Pinenq, M. A. Winnik, Effect of cross-linking on polymer diffusion in poly(butyl methacrylate-co-butyl acrylate) latex films. *Macromolecules* **32**, 6102–6110 (1999).
22. H. Y. Tai, D. Howard, S. Takae, W. Wang, T. Vermonden, W. E. Hennink, P. S. Stayton, A. S. Hoffman, A. Endruweit, C. Alexander, S. M. Howdle, K. M. Shakesheff, Photo-cross-linked hydrogels from thermoresponsive PEGMEMA-PPGMA-EGDMA copolymers containing multiple methacrylate groups: Mechanical property, swelling, protein release, and cytotoxicity. *Biomacromolecules* **10**, 2895–2903 (2009).
23. J. P. Lorand, J. O. Edwards, Polyol complexes and structure of the benzeneboronate ion. *J. Org. Chem.* **24**, 769–774 (1959).
24. A. G. Gomes, A. M. Azevedo, M. R. Aires-Barros, D. M. F. Prazeres, Studies on the adsorption of cell impurities from plasmid-containing lysates to phenyl boronic acid chromatographic beads. *J. Chromatogr. A* **1218**, 8629–8637 (2011).
25. A. Matsumoto, T. Ishii, J. Nishida, H. Matsumoto, K. Kataoka, Y. Miyahara, A synthetic approach toward a self-regulated insulin delivery system. *Angew. Chem. Int. Ed. Engl.* **51**, 2124–2128 (2012).
26. G. J. Chen, Z. Chen, D. Wen, Z. Wang, H. Li, Y. Zeng, G. Dotti, R. E. Wirz, Z. Gu, Transdermal cold atmospheric plasma-mediated immune checkpoint blockade therapy. *Proc. Natl. Acad. Sci. U.S.A.* **117**, 3687–3692 (2020).
27. O. Wintersteiner, H. A. Abramson, The isoelectric point of insulin: Electrical properties of adsorbed and crystalline insulin. *J. Biol. Chem.* **99**, 741–753 (1933).
28. R. H. Unger, Glucagon and the insulin: Glucagon ratio in diabetes and other catabolic illnesses. *Diabetes* **20**, 834–838 (1971).
29. J. Le Sauter, N. Geary, Pancreatic glucagon: Physiological signal of postprandial satiety. *Ann. Endocrinol. (Paris)* **54**, 149–161 (1993).
30. A. M. Arafat, M. O. Weickert, A. Adamidou, B. Otto, F. H. Perschel, J. Spranger, M. Möhlig, A. F. H. Pfeiffer, The impact of insulin-independent, glucagon-induced suppression of total ghrelin on satiety in obesity and type 1 diabetes mellitus. *J. Clin. Endocrinol. Metab.* **98**, 4133–4142 (2013).
31. A. Surnmerfield, F. Meurens, M. E. Ricklin, The immunology of the porcine skin and its value as a model for human skin. *Mol. Immunol.* **66**, 14–21 (2015).
32. X. Ye, Efficacy and safety of recombinant human insulin patch ZJSRM2021 (clinicaltrials.gov, 2021);https://clinicaltrials.gov/ct2/show/NCT05089942.
33. A. GhavamiNejad, J. Li, B. Lu, L. Zhou, L. Lam, A. Giacca, X. Y. Wu, Glucose-responsive composite microneedle patch for hypoglycemia-triggered delivery of native glucagon. *Adv. Mater.* **31**, e1901051 (2019).

Acknowledgments: We appreciate the help from G. Zhu (Cryo-EM center, Zhejiang University) for processing of samples for electron microscopy and D. Xu (Animal Center, Zhejiang University) for taking care of minipigs. **Funding:** This work was supported by the Fundamental Research Funds for the Central Universities (2021FZZX001-47 to Y.Z.), the Foundation of National Facility for Translational Medicine (Shanghai) (TMSK-2021-410 to Y.Z.), and the grants from the Startup Package of Zhejiang University to Z.G., J.Y., and Y.Z. **Author contributions:** Z.G., J.Y., Y.Z., C.Y., and T.S. proposed the conception of the project. C.Y., T.S., W.H., J.Z., L.C, H.W., W.L., S.W., and X.Y. performed all the experiments and collected the data. All the authors discussed the results and commented on the manuscript. **Competing interests:** Z.G., J.Y., Y.Z., C.Y., and X.Y. are inventors on a patent application related to this work filed by Zhejiang University (no. 202210552078.9, filed 18 May 2022). Z.G. is the cofounder of Zenomics Inc., Zencapsule Inc., Lizen Inc., Wskin Inc., and ZCapsule Inc. Z.G. and Y.Z. are the cofounders of Nantong μZen Pharmaceutical Technology Co. Ltd. The other authors declare that they have no competing interest. **Data and materials availability:** All data needed to evaluate the conclusions in the paper are present in the paper and/or the Supplementary Materials.

Submitted 3 June 2022
Accepted 15 October 2022
Published 30 November 2022
10.1126/sciadv.add3197